Hyperfine Structure of Oxygen Calculated by Many-Body Theory. II*

Hugh P. Kelly
Department of Physics, University of Virginia, Charlottesville, Virginia 22903
(Received 23 December 1968)

Many-body perturbation theory is used to calculate the contributions to the hyperfine structure of atomic oxygen from the orbital, spin-dipolar, and quadrupole interactions. The resulting values for $\langle r_l^{-3}\rangle$ and $\langle r_{sd}^{-3}\rangle$ are 4.56 a.u. and 5.170 a.u., respectively, which are in good agreement with those measured by Harvey. Our calculated value for $\langle r_q^{-3}\rangle$ is 4.216 a.u., which together with Harvey's measured value for b_2, leads to a nuclear quadrupole moment for O^{17} of -0.0263×10^{-24} cm^2.

I. INTRODUCTION

In his interesting study of the hyperfine structure (hfs) of O^{17}, Harvey[1] found that his experimental results could not be characterized by a single value of $\langle r^{-3}\rangle$ for a $2p$ electron. He found that different values $\langle r_l^{-3}\rangle$ and $\langle r_{sd}^{-3}\rangle$ were required for the orbital and spin-dipolar parts, respectively, of the hfs Hamiltonian. A third value $\langle r_q^{-3}\rangle$ is associated with the quadrupole hfs interaction. Bessis *et al.*[2] partially explained this effect by carrying out extensive configuration interaction calculations involving $s\rightarrow s'$ and $p\rightarrow p'$ excitations; but they obtained values for $\langle r_{sd}^{-3}\rangle/\langle r_l^{-3}\rangle$ which, although in the correct direction, were smaller than Harvey's result. This interesting effect was then explained by Judd[3] who emphasized the importance of $s\rightarrow d$ excitations in addition to $2p\rightarrow p'$ excitations. Judd carried out second-order calculations[3] and estimated the small relativistic corrections to obtain a value of 1.12 for $\langle r_{sd}^{-3}\rangle/\langle r_l^{-3}\rangle$ as compared with Harvey's value[1] of 1.13.

Schaefer, Klem, and Harris[4] have recently calculated accurate configuration interaction wave functions involving single excitations for the ground states of B, C, N, O, and F. They calculated the hfs constants for these atoms and found good agreement with experiment except for spin densities at the nucleus, which were too small.

In this paper, the many-body perturbation theory of Brueckner[5] and Goldstone[6] is applied to the calculation of the contribution to the hfs of oxygen from orbital, spin-dipolar, and quadrupole interactions. The contribution to the oxygen hfs from the Fermi contact interaction was recently calculated[7] by many-body theory and found to be in good agreement with Harvey's experimental result.[1] A detailed discussion of perturbation theory and hfs has been given by Sandars.[8] In order to apply the Brueckner-Goldstone perturbation expansion to atoms, we use the methods developed previously.[9–11] Our methods for applying many-body perturbation theory to atoms have also been utilized recently by Das and coworkers.[12,13]

Following Trees[14] and Bessis *et al.*,[2] we write the magnetic hyperfine constants $A(J,J')$ in the form

$$A(J,J')=2\beta_n\beta_e[\lambda_l(J,J')\alpha_l+\lambda_d(J,J')\alpha_d+\lambda_s(J,J')\alpha_s], \quad (1)$$

where β_n is the nuclear magnetic moment and β_e is the Bohr magneton. We are using the notation of Bessis, Lefebvre-Brion, and Moser.[2] The reduced matrix elements for the orbital, spin-dipolar, and Fermi contact interactions are given, respectively, by

$$\alpha_l=\langle LS\|\textstyle\sum_i \vec{l}_i/r_i^3\|LS\rangle, \quad (2)$$

$$\alpha_d=-\langle LS\left\|\sum_i \frac{\vec{s}_i}{r_i^3}-\frac{3\vec{r}_i(\vec{s}_i\cdot\vec{r}_i)}{r_i^5}\right\|LS\rangle, \quad (3)$$

and

$$\alpha_s=(8\pi/3)\langle LS\|\textstyle\sum_i \delta(r_i)\vec{s}_i\|LS\rangle. \quad (4)$$

The electric quadrupole hfs constant

$$b_J=-e^2Q\lambda_q(J,J)\alpha_q, \quad (5)$$

where Q is the nuclear electric quadrupole moment, and

$$\alpha_q=\langle LS\|\textstyle\sum_i (3\cos^2\theta_i-1)/r_i^3\|LS\rangle. \quad (6)$$

The values for λ for ^3P states are given by Bessis *et al.*[2] They also define the constants

$$a_J=(IJ)^{-1}A(J,J), \quad (7)$$

and

$$a_{J'}=I^{-1}(2J-1)^{-1/2}A(J,J-1). \quad (8)$$

In calculating the hfs constants, one must calculate the reduced matrix elements α_l, α_d, α_s, and α_q. In this paper we evaluated the matrix elements

$$\langle LS, M_L = L, M_S = S \left| \sum_{i=1}^{N} \frac{l_{zi}}{r_i^3} \right| LS, M_L = L, M_S = S \rangle$$

$$\equiv \langle r^{-3} \rangle_{\mathrm{HF}} (1 + \gamma_l), \tag{9}$$

$$\langle LS, M_L = L, M_S = S \left| \sum_{i=1}^{N} \frac{2 s_{zi} C_0^{(2)}(\theta_i, \phi_i)}{r_i^3} \right|$$

$$\times | LS, M_L = L, M_S = S \rangle \equiv \tfrac{1}{5} \langle r^{-3} \rangle_{\mathrm{HF}} (1 + \gamma_{sd}), \tag{10}$$

and

$$\langle LS, M_L = L, M_S = S \left| \sum_{i=1}^{N} \frac{C_0^{(2)}(\theta_i, \phi_i)}{r_i^3} \right|$$

$$\times | LS, M_L = L, M_S = S \rangle \equiv -\tfrac{1}{5} \langle r^{-3} \rangle_{\mathrm{HF}} (1 + \gamma_q), \tag{11}$$

where

$$C_q^{(k)}(\theta, \phi) = [4\pi/(2k+1)]^{1/2} Y_{kq}(\theta, \phi), \tag{12}$$

and $$\langle r^{-3} \rangle_{\mathrm{HF}} = \int_0^\infty (P_{2p}^{\,2}/r^3) dr, \tag{13}$$

with $P_{2p}(r)$ being the restricted Hartree-Fock $2p$ orbital (times r). We note that $C_0^{(2)}(\theta, \phi) = \frac{1}{2}(3 \times \cos^2\theta - 1)$. The corrections γ_l, γ_{sd}, and γ_q are then the corrections due to use of a restricted Hartree-Fock wave function.

In the case of the spin-dipolar interaction of Eq. (10), the z component is actually given by[15]

$$-\left(\frac{\vec{s}}{r^3} - \frac{3\vec{r}(\vec{r} \cdot \vec{s})}{r^5} \right)_z = -\frac{10^{1/2}}{r^3} \sum_{q_1, q_2} s(1, q_1)$$

$$\times C_{q_2}^{(2)}(\theta, \phi)(1 q_1 2 q_2 | 1210). \tag{14}$$

Since in Eq. (10) we are calculating the diagonal matrix element of the interaction and since we have a well defined M_L and M_S, there is no contribution from the terms $s(1, \pm 1)$ of Eq. (14). The Clebsch-Gordan coefficient[15] $(1020|1210) = -(2/5)^{1/2}$, and we obtain the simplified form of the spin-dipolar operator used in Eq. (10). Using the Wigner-Eckart theorem[15] the reduced matrix elements of Eqs. (2), (3), and (6) may be readily obtained from the matrix elements of Eqs. (9)–(11). In the following section results are given for γ_l, γ_{sd}, and γ_q. The result for α_s was presented previously.[7]

II. NUMERICAL RESULTS

As discussed in our previous hyperfine calculation,[7] the matrix elements of Eqs. (9)–(11) may be evaluated by calculating all linked energy terms or linked diagrams[5,6] which are first order in the appropriate hyperfine interaction, but contain any number of interactions with the Coulomb perturbation $\sum v_{ij} - \sum V_i$, where V is the potential used to calculate the single-particle states. In first order, γ_l, γ_{sd}, and γ_q are zero, and we obtain the restricted Hartree-Fock result.

Calculations of the terms in the perturbation expansion were carried out by use of the methods described previously.[9–11] The sums over bound states were carried out explicitly to a large value of the principal quantum number (usually about ten), and the remaining bound states were included by the n^{-3} rule.[10] Sums over continuum states were carried out by numerical integration.

Diagrams corresponding to the second-order perturbation terms are given in Fig. 1(a)–(c). The crossed interaction in Fig. 1(c) represents the net effect of interactions with the passive unexcited states and with the potential $-V$. In the usual many-body notation,[6] the crossed interaction represents only interaction with $-V$. Diagram 1 (d) shows an insertion on the hole line due to the net interaction with the passive unexcited states and with $-V$. There are also diagrams with similar insertions on the particle line. Inclusion of all these diagrams yield what we call the shifted second-order results. The inclusion of these interactions on the $1s$ hole line shifts the ϵ_{1s} to become very nearly the Hartree-Fock value; this shifted ϵ_{1s} is used for our second-order results and in all our calculations. This technique is discussed in detail in Ref. 10. The triangular interaction in Fig. 1 represents interaction with

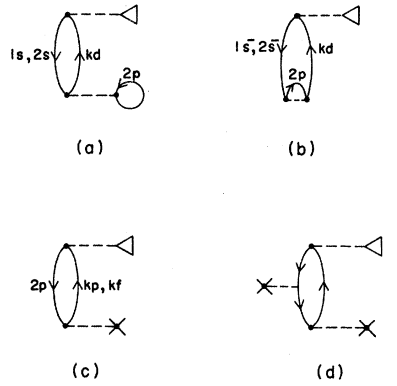

FIG. 1. (a), (b), and (c) are Brueckner-Goldstone diagrams contributing to the second-order hfs result. The triangular symbol indicates the hfs interaction. In diagram (c), the crossed interaction represents the net effect of interactions with passive unexcited states and with $-V$. (d) Third-order diagram which modifies the second-order results. The interaction may also occur on the particle line. All above diagrams also occur inverted.

one of the hyperfine operators listed in Eqs. (9)–(11). The operator is chosen according to which matrix element we are calculating.

Results due to the second-order diagrams of Fig. 1(a)–(c) are listed in Table I. We note that the relation between $\langle r^{-3}\rangle$ and γ is given by

TABLE I. Second-order results. Bound and continuum excited states are included. In the calculations, the value used for ϵ_{1s} is the shifted value given in Ref. 7 which includes the effects of Fig. 1(d) on the 1s hole line.

	γ_l	γ_{sd}	γ_q
$2s\rightarrow kd$[a]	0.000 00	0.000 00	−0.016 87
$2s\rightarrow kd$[b]	0.000 00	0.015 43	0.015 43
$1s\rightarrow kd$[a]	0.000 00	0.000 00	−0.051 46
$1s\rightarrow kd$[b]	0.000 00	0.028 32	0.028 32
$2p\rightarrow kp$	−0.046 03	−0.009 21	−0.082 86
$2p\rightarrow kf$	0.000 00	0.013 08	−0.013 08
Total	−0.046 03	0.047 63	−0.120 52

[a]From diagram of Fig. 1(a). [b]From diagram of Fig. 1(b).

$$\langle r_l^{-3}\rangle = \langle r^{-3}\rangle_{\mathrm{HF}}(1+\gamma_l), \tag{15}$$

$$\langle r_{sd}^{-3}\rangle = \langle r^{-3}\rangle_{\mathrm{HF}}(1+\gamma_{sd}), \tag{16}$$

and

$$\langle r_q^{-3}\rangle = \langle r^{-3}\rangle_{\mathrm{HF}}(1+\gamma_q). \tag{17}$$

Through second-order, we obtain (in a.u.)

$$\langle r_l^{-3}\rangle = 4.746, \quad \langle r_{sd}^{-3}\rangle = 5.212,$$

and $\langle r_q^{-3}\rangle = 4.375$.

We have used $\langle r^{-3}\rangle_{\mathrm{HF}} = 4.9750$ a.u. which resulted from our restricted Hartree-Fock calculation. Harvey's experimental result[1] for $\langle r_l^{-3}\rangle = 4.58$ and for $\langle r_{sd}^{-3}\rangle = 5.19$. Our second-order result for $\langle r_{sd}^{-3}\rangle$ is in excellent agreement with experiment, but our second-order value for $\langle r_l^{-3}\rangle$ is only in fair agreement with experiment. Approximately one-third of the contributions from 2s and 2p excitations was from bound excited states. Diagram 1(a) contributes only to γ_q, and γ_l is determined (in second order) by diagram 1(c) with kp excitations only.

Since we only include one hyperfine interaction, in the next order of perturbation theory we consider terms with two interactions with the Coulomb perturbation $\sum v_{ij} - \sum V_i$ in addition to the hfs interaction. Typical third-order diagrams are shown in Figs. 2–4. However, all third-order diagrams were calculated. The diagrams of Fig. 2 are referred to as polarization diagrams. They contain one interaction with passive unexcited states or

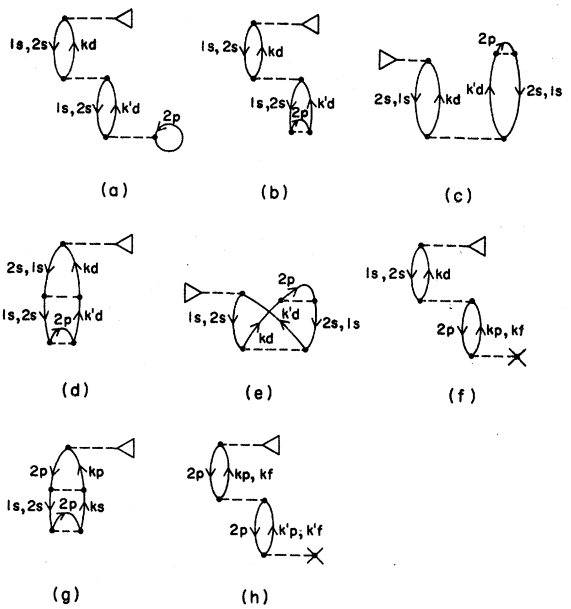

FIG. 2. Typical third-order polarization diagrams. These involve one interaction with passive unexcited states or with $-V$.

with $-V$. Results of the polarization diagrams are listed in the first row of Table II. The diagrams of Fig. 3 are correlation diagrams in which one of the hole states is 1s or 2s, and one of the excited states is $2p$ (0^- or -1^-).

Exchange diagrams are not shown but were included in the calculations. The contribution of the diagrams of Fig. 3 to γ_l, γ_{sd}, and γ_q are listed in Table II.

In Fig. 4 are shown the remaining types of third-order diagrams and their contributions are listed in Table II. Again, the exchange diagrams

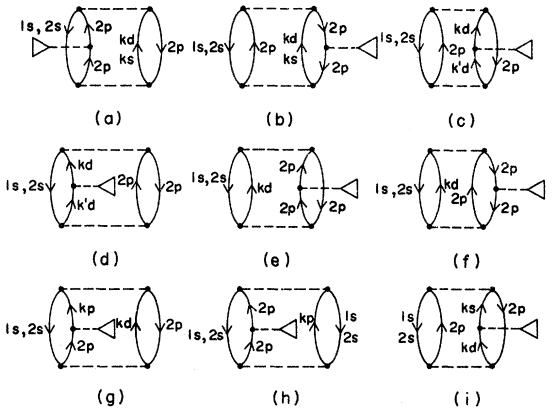

FIG. 3. Additional third-order diagrams which involve correlations. Exchange diagrams are also included in the calculations. Diagrams (g) and (i) also occur inverted.

are included in the calculations although not drawn in Fig. 4. In Fig. 4(a) the k,k' excitations do not include the $2p$ excited states since these were included in the diagrams of Fig. 3. Also, the hyperfine interaction may occur on the particle lines k or k'. Similarly, in 4(b) the hfs interaction may occur on the other hole line or on the particle lines. Diagrams (c) to (g) also occur inverted. Diagrams (e) and (f) were found to be individually large, but are of opposite sign, and the sum listed in Table II is rather small. We note that 4(f) is an exclusion-principle-violating (EPV) diagram.[9] Diagrams 4(h)–(l) each involve two crossed interactions, the crossed interaction representing the net interaction with the passive unexcited states and with $-V$. The diagrams of the type shown in Fig. 1(d) also contribute to the third-order results. However, we consider them separately since many of these diagrams are accounted for by calculating the second-order results with a shifted energy denominator.[11] We are then also including some effects from fourth and higher orders.

If we now consider the second-order results of Table I and the third-order results of Table II, we obtain: $\langle r_l^{-3}\rangle = 4.577$, $\langle r_{sd}^{-3}\rangle = 5.089$, and $\langle r_q^{-3}\rangle = 4.152$. The value for $\langle r_l^{-3}\rangle$ is now in close agreement with experiment, but $\langle r_{sd}^{-3}\rangle$ does not agree as well with experiment as in second order.

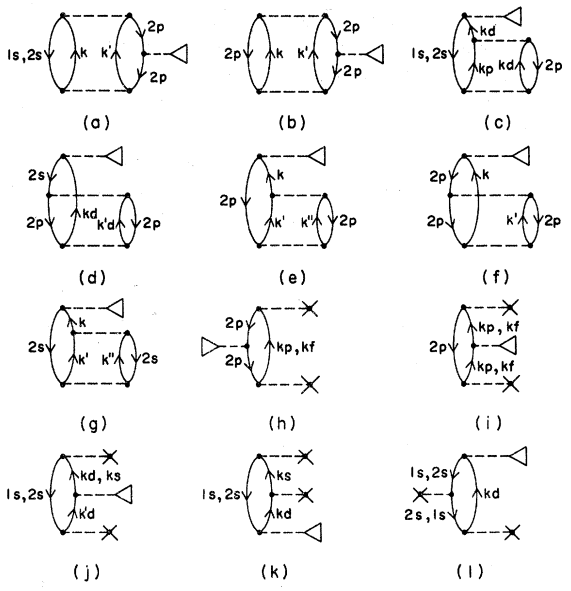

FIG. 4. Additional third-order diagrams. Calculations also include exchange diagrams. (a) does not include $2p$ excited states since these are given explicitly in Fig. 3. Interactions may also occur on the particle lines. (b) Interactions may occur on the other hole line and on the particle lines. (c) through (g) also occur inverted. (c) includes the $2p$ excited states. (f) is an EPV diagram according to Ref. 9.

In Table III are listed the "modified" second-order results. These results include the contributions from second-order diagrams, and also the diagrams like Fig. 1(d) and higher-order diagrams of this type. Table III also contains a summary of the third-order results and estimated and calculated results of many higher-order diagrams.

In Fig. 5 are shown some of the typical higher-order terms which were considered. These same types of diagrams were found important in the calculation of the contact interaction.[7] Diagrams 5(a) and (b) are fourth-order polarization diagrams. Contributions from fourth- and higher-order polarization diagrams were estimated and are listed in Table III. The effects of three-body and higher diagrams were also considered. A typical three-body diagram is shown in Fig. 5(c). Three-body diagrams were calculated in our previous oxygen hfs contact calculation.[7] Results of that calculation have been used to estimate the effects of three-body and higher diagrams for the present work. This estimated contribution is listed in Table III.

In Ref. 7, the diagrams we called "renormal-

TABLE II. Third-order results. All exchange diagrams are also included. Diagrams of Fig. 1(d) are considered separately.

	γ_l	γ_{sd}	γ_q
Polarization diagrams[a]	−0.01789	−0.00675	−0.02175
Diagrams 3(a)–(f) plus exchange	−0.00882	−0.00925	−0.01175
Diagram 3(g)[b]	0.00094	0.00086	0.00114
Diagram 3(h)	−0.00044	−0.00044	−0.00062
Diagram 3(i)	0.00000	0.00011	−0.00013
Diagram 4(a)	−0.00016	−0.00044	−0.00044
Diagram 4(b) ($k'=2p$)	−0.00319	−0.00156	−0.00247
Diagram 4(b) (no excited $2p$ states)	−0.00359	−0.00420	−0.00676
Diagram 4(c)	0.00000	−0.00247	−0.00253
Diagram 4(d)	0.00000	0.00065	0.00127
Diagrams 4(e)+4(f)	0.00015	0.00015	0.00015
Diagram 4(g)	0.00000	0.00003	−0.00022
Diagrams 4(h)+4(i)	−0.00094	−0.00143	−0.00044
Diagrams 4(j), (h), (l)	0.00000	0.00008	−0.00033
Total	−0.03394	−0.02466	−0.04488

[a]Typical polarization diagrams are shown in Fig. 2. All third-order polarization diagrams are included in this result.

[b]The inverted diagram is also included in numerical results.

TABLE III. Inclusion of higher-order diagrams.

Diagrams	γ_l	γ_{sd}	γ_q
Modified second-order[a]	−0.050 48	0.043 54	−0.123 46
Third-order[b]	−0.033 94	−0.024 67	−0.044 88
Higher polarization[c]	−0.011 40	0.002 10	−0.003 80
Three-body[d]	0.005 20	0.006 50	0.007 60
Renormalization[e]	0.004 50	0.002 80	0.009 80
Total	−0.086 12	0.030 26	−0.154 74

[a]Includes diagrams like Fig. 1(d) and higher-order diagrams of this type in addition to second-order diagrams.

[b]All third-order diagrams except for those of Fig. 1 (d).

[c]Estimated contribution from fourth-order and higher-order polarization diagrams; examples shown in Fig. 5 (a) and (b).

[d]Estimated contribution from correlation diagrams with three or more different hole states. Typical diagram shown in Fig. 5(c).

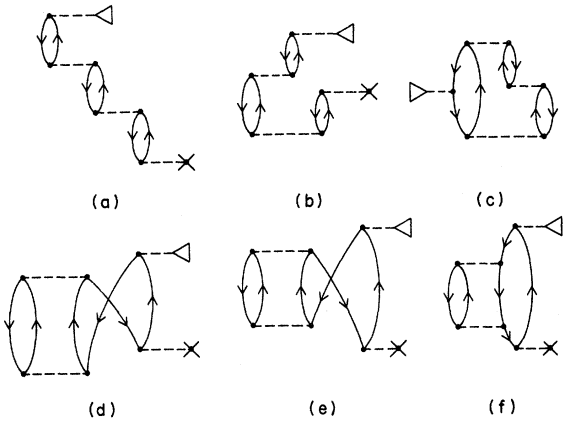

FIG. 5. Typical higher-order diagrams contributing to hyperfine structure. Diagrams (a) and (b) are fourth-order polarization diagrams. (c) Typical three-body diagram. The hfs interaction may also occur on the other hole lines or on the particle lines. (d), (e), and (f) are renormalization diagrams which modify the basic diagrams of Fig. 1.

ization" diagrams were found to be quite important. Several of the renormalization diagrams are shown in Fig. 5(d)–(f); and they are all listed in Fig. 5 of Ref. 7. These diagrams modify the basic second-order diagrams of Fig. 1. Our value for the contribution from the renormalization diagrams is given in Table III, and they are not so important as in Ref. 7. At the bottom of Table III are our final values for γ_l, γ_{sd}, and γ_q before the inclusion of relativistic corrections.

In Table IV are listed the results for $\langle r_l^{-3}\rangle$, $\langle r_{sd}^{-3}\rangle$, and $\langle r_q^{-3}\rangle$. The third row contains our

TABLE IV. Results for $\langle r^{-3}\rangle$ in a.u. (Our calculated restricted Hartree-Fock value is 4.9750 a.u.).

	$\langle r_l^{-3}\rangle$	$\langle r_{sd}^{-3}\rangle$	$\langle r_q^{-3}\rangle$
Second order	4.746	5.212	4.375
From Table III. This work with relativistic corrections[a]	4.563	5.170	4.216
Schaefer *et al.*[b]	4.613	5.125	4.334
Bessis *et al.*[d]	4.68	4.89	4.56
Experiment (Harvey[i])	4.58	5.19	

[a]Correction factors of 1.0035 and 1.0086 for $\langle r_l^{-3}\rangle$ and $\langle r_{sd}^{-3}\rangle$, respectively, are taken from B. R. Judd, Ref. 3. An approximate correction of 1.0027 for $\langle r_q^{-3}\rangle$ has been taken from Ref. 16.

[b]Reference 4. Relativistic corrections not included.

[c]Configuration interaction result of Ref. 2. Relativistic corrections not included.

results for $\langle r^{-3}\rangle$ multiplied by relativistic corrections. For $\langle r_l^{-3}\rangle$ and $\langle r_{sd}^{-3}\rangle$, we have multiplied by the factors 1.0035 and 1.0086, respectively, which were taken from Judd.[3] For $\langle r_q^{-3}\rangle$, an approximate relativistic correction of 1.0027 was obtained from Kopfermann.[16] In Table IV our results are compared with those of Schaefer *et al.*,[4] with those of Bessis *et al.*,[2] and with Harvey's experimental results.[1] Our results are quite close to those of Schaefer *et al.* Since the results of Schaefer *et al.*[4] and of Bessis *et al.*[2] do not include relativistic corrections, they should be compared with our results before the relativistic corrections are included. Bessis *et al.*[2] have calculated the $\langle r^{-3}\rangle$ values by various approximations and it is their CI (configuration interaction) result which is listed in Table IV.

In Table V we have listed our calculated values for a_2 and a_1, and we compare with the results of Schaefer *et al.*[4] and with experiment.[2,17] Our values for the nuclear magnetic dipole moments are taken from Fuller and Cohen.[18] In the O^{15} experiment, Commins and Feldman[17] give only a result for a_2. In calculating a_2 and a_1, the value of $\langle r^{-3}\rangle$ with relativistic corrections were taken from Table IV. The value for the Fermi contact term α_s was taken from Ref. 7 and was reduced by a relativistic correction of two percent as suggested by Judd.[3] The constants a_2' and a_1' have also been calculated in this work to be −128.04 Mc/sec and −87.5 Mc/sec, respectively, as compared with the experimental values −127.5 ± 2 Mc/sec and −91.7 ± 7.2 Mc/sec.

We have also calculated the nuclear quadrupole moment Q using the value for $\langle r_q^{-3}\rangle$ of 4.216 a.u. from Table IV and making use of Harvey's[1] value $b_2 = -10.438$ Mc/sec. Our resulting value for Q for O^{17} is -0.02634×10^{-24} cm^2.

TABLE V. Hyperfine constants in Mc/sec.

	$a_2(O^{17})$	$a_1(O^{17})$	$a_2(O^{15})$	$a_1(O^{15})$
This work[a]	−220.075	4.105	417.73	−7.792
Schaefer *et al.*[b]	−212.966	9.257	404.24	−17.571
Experiment	−219.61[c] ± 0.05	4.738[c] ± 0.036	414.87[d]	

[a]We have used our previous value for $|\psi(0)|^2$ calculated in Ref. 7 and then used a two percent relativisitc correction as estimated by Judd in Ref. 3.

[b]Taken from Ref. 4. If the relativistic corrections are applied, these results are brought into closer agreement with experiment.

[c]From Ref. 1. This value corrected by Harvey for a slight breakdown of LS coupling.

[d]From Ref. 17. No result for a_1 for O^{15} is given.

III. DISCUSSION AND CONCLUSIONS

These calculations illustrate the utility of many-body perturbation theory in correcting Hartree-Fock wave functions. Although our second-order results are reasonable, we have found significant contributions from higher-order terms. In obtaining our final results, we estimated the effects of three-body and higher terms as shown in Fig. 5(c). Our estimated contributions are believed to be fairly reliable since these terms were explicitly calculated in the Fermi contact calculation.[7] As a result of estimating these terms and also the higher-order polarization terms as shown in Fig. 5(a) and (b), our final results for γ_l, γ_{sd}, and γ_q in Table III are probably accurate to about 90%. The resulting uncertainty in $\langle r_l^{-3}\rangle$ is less than 1%; for $\langle r_{sd}^{-3}\rangle$, it is approximately 0.3%; and for $\langle r_q^{-3}\rangle$, it is approximately 1.5%. Our value for $Q(O^{17}) = -0.0263\times10^{-24}$ cm^2 is rather close to the value -0.0256×10^{-24} cm^2 obtained by Schaefer *et al.* Previous results for $Q(O^{17})$ include the values -0.024×10^{-24} cm^2 obtained by Bessis[2] *et al.*, -0.026×10^{-24} cm^2 obtained by Stevenson and Townes,[19] and -0.0265×10^{-24} cm^2 obtained by Kamper, Lea, and Lustig.[20] The result by Kamper, Lea, and Lustig,[20] contains the Sternheimer correction[21] for polarization of the inner electrons. The present many-body calculation includes the Sternheimer corrections in the second-order terms.

In comparing with the results of Schaefer, Klemm, and Harris,[4] their values for $\langle r_l^{-3}\rangle$ and $\langle r_{sd}^{-3}\rangle$ are essentially as close to experiment[2] as those of this calculation, particularly if the relativistic corrections are applied to their results. Our closer agreement with the experimental hfs constants given in Table V is mostly due to our improved value for $|\psi(0)|^2$. Although Schaefer *et al.* state that they have only included single excitations, it appears that, in our terminology, they have also included double excitations in which one of the excited states is a $2p$ (0^- or -1^-) excited state. They have then included such correlation terms as are shown in Fig. 3 or Fig. 4(b) when k or k' equals $2p$. This is also checked by noting that the amount of correlation energy obtained by Schaefer *et al.* is very close to that obtained in Ref. 7 from $2s2p \rightarrow 2p(0^-, -1^-)kd$ excitations. The present calculation also contains many terms and effects not included by Schaefer *et al.*, but it is interesting to note that in this case there has been much cancellation among these higher-order terms and our results are close to those of Schaefer *et al.*[4] This, however, is not true in the case of the contact interaction.[7]

Many-body perturbation theory appears to be useful in calculating hyperfine structure as well as other properties. There always remains the problem of calculating higher-order terms to greater accuracy; and the three-body and higher diagrams may be of increasing importance in larger atoms. These and other problems will be investigated in future work.

ACKNOWLEDGMENTS

I wish to thank Professor J. S. M. Harvey, Professor Brian R. Judd, and Professor P. G. H. Sandars for very helpful discussions. I also wish to thank Dr. H. F. Schaefer and Dr. J. D. Lyons for preprints of their work.

*Research sponsored in part by the Aerospace Research Laboratories, Office of Aerospace Research, United States Air Force, Contract No. F33615-69-C-1048, and by the U. S. Atomic Energy Commission, Document ORO-2915-96.

[1]J. S. M. Harvey, Proc. Roy. Soc. (London) A285, 581 (1965).

[2]N. Bessis, H. Lefebvre-Brion, and C. M. Moser, Phys. Rev. 128, 213 (1962).

[3]B. R. Judd, in La Structure Hyperfine des Atomes

et des Molecules, edited by R. Lefebvre and C. Moser (Editions du Centre National de la Recherche Scientifique, Paris, 1967), p. 311.

[4]H. F. Schaefer III, R. A. Klemm, and F. E. Harris, Phys. Rev. 176, 49 (1968).

[5]K. A. Brueckner, Phys. Rev. 97, 1353 (1955); 100, 36 (1955); The Many-Body Problem (John Wiley & Sons, Inc., New York, 1959).

[6]J. Goldstone, Proc. Roy. Soc. (London) A239, 267 (1957).

[7]H. P. Kelly, Phys. Rev. 173, 142 (1968).

[8]P. G. H. Sandars, in La Structure Hyperfine des Atomes et des Molecules, edited by R. Lefebvre and C. Moser (Editions du Centre National de la Recherche Scientifique, Paris, 1967), p. 111; Advan. Chem. Phys. (to be published).

[9]H. P. Kelly, Phys. Rev. 131, 684 (1963).

[10]H. P. Kelly, Phys. Rev. 136, B896 (1964).

[11]H. P. Kelly, Phys. Rev. 144, 39 (1966).

[12]E. S. Chang, R. T. Pu, and T. P. Das, Phys. Rev. 174, 1 (1968).

[13]J. D. Lyons, R. T. Pu, and T. P. Das, to be published.

[14]R. E. Trees, Phys. Rev. 92, 308 (1953).

[15]A. R. Edmonds, Angular Momentum in Quantum Mechanics (Princeton University Press, Princeton, New Jersey, 1960), p. 118.

[16]H. Kopfermann, Nuclear Moments (Academic Press, Inc., New York, 1958).

[17]E. D. Commins and H. R. Feldman, Phys. Rev. 131, 700 (1963).

[18]G. H. Fuller and V. W. Cohen, Nuclear Data Sheets, compiled by K. Way *et al.* (Printing and Publishing Office, National Academy of Sciences – National Research Council, Washington 25, D.C.), Appendix I.

[19]M. J. Stevenson and C. H. Townes, Phys. Rev. 107, 635 (1957).

[20]R. A. Kamper, K. R. Lea, and C. D. Lustig, Proc. Phys. Soc. 70B, 897 (1957).

[21]R. M. Sternheimer, Phys. Rev. 86, 316 (1952).

PHYSICAL REVIEW VOLUME 180, NUMBER 1 5 APRIL 1969

Intensity and Gain Measurements on the Stimulated Raman Emission in Liquid O_2 and N_2†

J. B. Grun,* A. K. McQuillan,‡ and B. P. Stoicheff
Department of Physics, University of Toronto, Toronto 5, Canada
(Received 25 November 1968)

In liquid O_2 and N_2 the threshold for stimulated Raman emission is found to be much lower than for other nonlinear processes. Thus it is possible to make reliable measurements of the intensity of Raman emission over a large range of incident laser power by using a simple longitudinal geometry. Several distinct regions of emission were investigated, including normal Raman scattering, exponential gain, onset of oscillation, and saturation. There is good agreement with theory.

INTRODUCTION

It is well known[1–3] that the comparison of theoretical and experimental values of intensity and gain in stimulated Raman emission is complicated by several competing processes such as self-focusing, and Brillouin and Rayleigh scattering, all of which may have similar appearance thresholds. Thus, anomalous intensity behavior in many liquids and even in gases[4–6] and solids[7] appears to be the rule rather than the exception. One important consequence is that the premature onset of oscillation has precluded the observation of the expected exponential gain in most materials, with the exception of gaseous hydrogen, liquid acetone, and carbon tetrachloride.[8] Bloembergen and Lallemand[3,6] have overcome some of these difficulties by the use of a Raman amplifier and have demonstrated its importance in obtaining reliable values of the Raman gain. Other useful experimental arrangements in such studies include the transverse resonator of Dennis and Tannenwald,[9] the off-axis resonator of Jennings and Takuma,[10] and the diffusely pumped amplifier of Bortfeld and Sooy.[11] More recently, Shapiro, Giordmaine, and Wecht,[12] Bret and Weber,[13] and Kaiser and Maier[14] have shown that with picosecond and subnanosecond laser pulses stimulated Raman scattering is the dominant nonlinear scattering process in several liquids, and thus have obtained good agreement